CLM-R 133

UKAEA RESEARCH GROUP

Report

COMPUTATION OF MHD EQUILIBRIA IN TOKAMAK

C LI THOMAS
F A HAAS

CULHAM LABORATORY
Abingdon Berkshire
1974

Available from H. M. Stationery Office

C.18

PRICE 50p

CLM-R 133

U.D.C.
621.039.61.026 TOKAMAK
538.4 : 681.3

COMPUTATION OF MHD EQUILIBRIA IN TOKAMAK

by

C. Ll. Thomas and F.A. Haas

A B S T R A C T

A code (TOPE) has been written to study MHD equilibria in Tokamak. We consider four different models of the equilibrium and describe the numerical techniques appropriate to each. Where possible, asymptotic analysis has been developed, and used (a) to elucidate the qualitative features of the models, and (b) to check the code. The results are presented as a series of examples.

UKAEA Research Group,
Culham Laboratory,
Abingdon,
Berks.

January 1974

SBN: 85311 025 5

1. INTRODUCTION

We investigate magnetohydrodynamic equilibria in Tokamak. Our objective is to consider different models of equilibrium and to develop numerical methods of solution appropriate to each physical situation. These techniques should be of use, both in design work for future experiments, and in obtaining equilibria for numerical magnetohydrodynamic stability studies.

It is well known that by defining a poloidal-flux ψ, such that the poloidal magnetic field is given by

$$\underline{B} = \frac{1}{R} \nabla\psi \times \underline{e}_\varphi , \qquad (1)$$

then the axisymmetric toroidal MHD equilibrium equation can be written in the form [1]

$$R \frac{\partial}{\partial R}\left(\frac{1}{R}\frac{\partial \psi}{\partial R}\right) + \frac{\partial^2 \psi}{\partial Z^2} = -Rj_\varphi = -FF'(\psi) - R^2 p'(\psi) , \qquad (2)$$

where R, φ and Z are cylindrical coordinates based on the axis of symmetry, and F and p are arbitrary functions of ψ. In the present work, a finite difference code, TOPE (Toroidal Plasma Equilibrium)*, has been written to solve Eq. (2). The difference equations used are derived in the standard way, as described by Thomas[2]. The precise numerical procedure adopted depends on the physical model studied - in particular, whether or not a trivial solution can occur. Since the basic method is iterative, convergence difficulties might be anticipated. In the range of models considered here, however, this problem has not been encountered.

In principle, Eq. (2) can be solved for any choice of $F(\psi)$ and $p(\psi)$. In practice, however, the forms for F and p will be determined by the underlying diffusion process. Thus, for example, Grad and Hogan[3] have considered the simplest classical model for resistive diffusion in a Tokamak. Assuming the duration time of an experiment to be long compared with the diffusion time, they show the plasma to approach a unique limiting profile (and unique β) which is independent of the value of resistivity. Grad and Hogan infer that this profile will be established irrespective of the dissipative mechanism (classical or anomalous). The corresponding forms for p and F^2 are linear in ψ, and it follows that the equilibrium equation to be solved is linear and inhomogeneous.

In the present work, in order to study different physical situations, we consider a variety of forms for p and F. The work of Grad and Hogan suggests that for linear forms, at least, the results obtained from Eq. (2) should provide a plausible description of a Tokamak in "equilibrium".

The models considered are maintained in equilibrium by a perfectly conducting wall, and calculations have been made both with a wall touching the plasma (diffuse equilibrium), and with a wall away from the plasma (plasma-vacuum equilibrium). In all models we take the pressure to vanish at the boundary. The models for diffuse equilibria are characterised by the values of toroidal current density (j_φ) and pressure-gradient ($|\nabla p|$) prescribed at the boundary, namely, (a) $|\nabla p|$, j_φ finite (Model I), (b) $|\nabla p| = 0$, j_φ finite (Model II), and (c) $|\nabla p| = j_\varphi = 0$ (Model III). For a plasma-vacuum equilibrium we take $|\nabla p| = j_\varphi = 0$ at the interface (Model IV).

The chosen forms for p and F lead to phenomena such as bifurcation in Model II, and "eigenfunction" behaviour in Model III. Due to the number of parameters involved we make no attempt to optimise our models, but rather present the results as a series of examples.

2. MODEL I

We consider a diffuse equilibrium with $p(\psi)$ and $F(\psi)$ given by

$$p(\psi) = \frac{a\,\psi_B^2}{n\,R_o^4}\left(1 - \left(\frac{\psi}{\psi_B}\right)^n\right) \qquad (3)$$

and

$$F(\psi) = \left(C + \frac{2\,da\,\psi_B^2}{m\,R_o^2}\left(1 - \left(\frac{\psi}{\psi_B}\right)^m\right)\right)^{\frac{1}{2}} \qquad (4)$$

where ψ_B is the value of the poloidal-flux, ψ, at the boundary, and R_o is the major radius of the torus. The parameters C, a and d are free, but because of the form for F, Eq. (2) only involves the dimensionless quantities a and d. However, the toroidal field, $B_\varphi (= F(\psi)/R)$, does depend on C. With the above forms the toroidal current density and pressure gradient are non-vanishing at the boundary. The equation to be solved is linear or non-linear depending on the values prescribed to the integers n and m. Gourdon and Touche[4] have also solved the linear problem but with different forms from those given in (3) and (4). An important physical quantity to be evaluated is the poloidal-β, β_I, which throughout this report we define to be

$$\beta_I = \frac{8\pi \iint p\,dRdZ}{\left[\iint j_\varphi dRdZ\right]^2} , \qquad (5)$$

where the integrals are taken over the cross-sectional area.

For an equilibrium with circular cross-section it is straightforward to obtain an asymptotic solution in terms of the inverse aspect ratio, ϵ. This is useful because it enables us, (a) to elucidate the qualitative features to be expected, and (b) to check the numerical procedure.

(i) Asymptotic Analysis

Transforming to local polar coordinates r, θ, φ based on the centre of the minor cross-section (see Fig. 1), Eq. (2) can be written as

$$\frac{1}{r}\frac{\partial}{\partial r}\left(r\frac{\partial \psi}{\partial r}\right) + \frac{1}{r^2}\frac{\partial^2 \psi}{\partial \theta^2} - \frac{\cos\theta}{R_o + r\cos\theta}\frac{\partial \psi}{\partial r} + \frac{\sin\theta}{r(R_o + r\cos\theta)}\cdot\frac{\partial \psi}{\partial \theta}$$

$$+ FF'(\psi) + (R_o + r\cos\theta)^2 p'(\psi) = 0 . \qquad (6)$$

Substituting from Eqs. (3) and (4) and introducing the dimensionless variables $r \equiv r/r_o$ and $\Psi \equiv \psi/\psi_B$, Eq. (6) becomes

$$\frac{1}{r}\frac{\partial}{\partial r}\left(r\frac{\partial \Psi}{\partial r}\right) + \frac{1}{r^2}\frac{\partial^2 \Psi}{\partial \theta^2} - \frac{\epsilon\cos\theta}{1 + \epsilon r\cos\theta}\cdot\frac{\partial \Psi}{\partial r} + \frac{\epsilon\sin\theta}{r(1 + \epsilon r\cos\theta)}\cdot\frac{\partial \Psi}{\partial \theta}$$

$$- a\epsilon^2\left[d\Psi^{m-1} + (1 + \epsilon r\cos\theta)^2\,\Psi^{n-1}\right] = 0 , \qquad (7)$$

where $\epsilon = r_o/R_o$. We assume the ordering $a\epsilon^2 \sim 1$ and $d + 1 \sim \epsilon$, the latter implying that d be negative. We further assume that $n + md \sim \epsilon$. Thus taking $m = 4$, $n = 3$,

---

* We remark that TOPE could easily be amended to solve the problem

$$L(\psi) = G(\psi, \underline{x}) ,$$

where L is a linear elliptic operator, and G is any function of ψ and the independent variable $\underline{x}$, but not the derivatives of ψ.

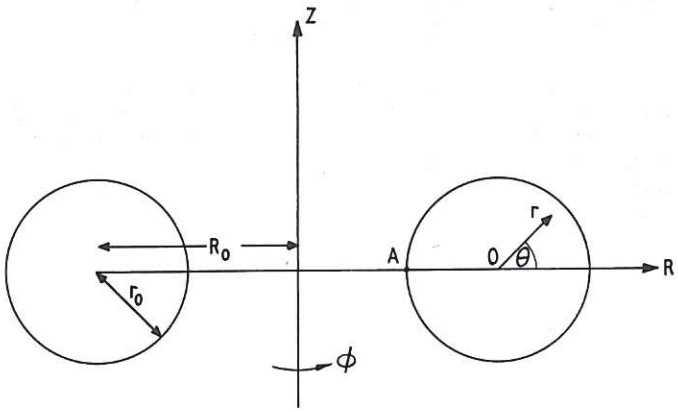

Fig. 1 Coordinate systems for a circular cross-section plasma.

$d = -0.8$ and $\epsilon = 0.2$, it follows that $n + md = -0.2$ and that our ordering is consistent. In fact, the numerical results reported in the next section demonstrate the asymptotic analysis to be valid over a wide range of parameters.

Expanding the solution in the form

$$\Psi = 1 + \Psi_1 + \dots , \tag{8}$$

we find Eq. (7) to be trivially satisfied in leading-order. To first order the appropriate solution ($\Psi_1 = 0$ at $r = 1$) is given by

$$\Psi_1 = -\frac{1}{4} a\epsilon^2(1+d)(1-r^2)(1+\nu r\cos\theta), \tag{9}$$

where $\nu = \epsilon(d+1)^{-1}$. This solution shows that the radial dependence of the pressure is essentially parabolic. The positions of the pressure maxima and minima, and hence the magnetic axes, are given by

$$3\nu r^2 + 2\mu r - \nu = 0 , \tag{10}$$

where $\mu = \pm 1$. Adam and Mercier[5] and Laval et al.[6] have derived equations of this type, but with different ν. For $0 < \nu < 1$ there is one (outward) magnetic axis corresponding to a pressure maximum. For $\nu > 1$ there are two magnetic axes, the second corresponding to an inward axis with a pressure minimum. For $-1 < \nu < 0$ there is one (inward) magnetic axis corresponding to a pressure minimum. For $\nu < -1$ there are again two magnetic axes, the second corresponding to an outward axis with a pressure maximum. Since p vanishes at the boundary the presence of a minimum implies the existence of a region of negative pressure. Thus the only case of practical interest is $0 < \nu < 1$, for which the displacement Δ of the magnetic axis can be written as

$$\Delta = \frac{1}{3\nu}\left[-1 + (1+3\nu^2)^{\frac{1}{2}}\right] . \tag{11}$$

It is straightforward to show, that to leading-order, the toroidal current density is given by

$$j_\varphi = \frac{a\epsilon^2}{R_o r_o^2}(1+d)(1+2\nu r\cos\theta)\,\psi_B . \tag{12}$$

We observe that the constant j_φ contours are perpendicular to the R-axis and parallel to the axis of symmetry. For $\nu = \frac{1}{2}$ the toroidal current density is zero at the innermost point of the torus, that is, point A in Fig. 1. Increasing ν above this value leads to a region of reversed current spreading into the plasma from this point. Using the above formulae, Eq. (5) leads to a very simple expression for the poloidal-β, namely

$$\beta_I = \frac{1}{1+d} = \frac{\nu}{\epsilon} . \tag{13}$$

Thus for a given ϵ the poloidal-β depends only on the parameter ν.

It is clear that the essential physical features of our model can be described in terms of ν. Thus as ν is increased j_φ remains unidirectional until $\beta_I = \beta_I^* = 0.5\,\epsilon^{-1}$, the critical value for current reversal. Increasing ν still further eventually leads to an upper limit for β_I. This is set by the second magnetic axis about to enter the plasma on the inside of the torus (point A in Fig. 1), and is given by $\beta_I = \beta_I^+ = \epsilon^{-1}$, the pressure maximum being displaced outwards a distance $\Delta = \frac{1}{3}$. We note that to the order of our theory, β_I is independent of 'a', although the poloidal flux, the magnitude of j_φ etc., do depend on this parameter.

(ii) Computations

Normalising R and Z with respect to R_o and defining the dimensionless flux $\Psi = \psi/\psi_B$, then Eq. (2) can be written as

$$R\frac{\partial}{\partial R}\left(\frac{1}{R}\frac{\partial\Psi}{\partial R}\right) + \frac{\partial^2\Psi}{\partial Z^2} - a[d\Psi^{m-1} + R^2\Psi^{n-1}] = 0, \tag{14}$$

where $\Psi = 1$ at the boundary. We have solved Eq. (14) with m, n in the range $2 \leq m \leq 5$ and $2 \leq n \leq 5$, for both circular and non-circular cross-section plasmas. The solution is used to evaluate the dimensionless toroidal current density

$$\frac{R_o^3 j_\varphi}{\psi_B} = -\frac{a}{R}(d\Psi^{m-1} + R^2\Psi^{n-1}) , \tag{15}$$

and hence the poloidal-β.

For $m = n = 2$, the equation is linear, and provided the eigenvalues of

$$R\frac{\partial}{\partial R}\left(\frac{1}{R}\frac{\partial}{\partial R}\right) + \frac{\partial^2}{\partial Z^2} - a(d + R^2)$$

are all negative, the equation has a unique solution. For other values of m and n, however, the equation is non-linear and the number of solutions to be expected is unclear. Since Eq. (14) is, in general, non-linear, it is appropriate to use Newton's method. Eq. (14) is of the type

$$L\Psi = f(\Psi, R) , \tag{16}$$

where L is the elliptic operator. For the purpose of discussion, however, we write Eq. (16) as

$$N(\Psi) = 0 . \tag{17}$$

Newton's method applied to this equation is

$$N'(\Psi^n)\Delta\Psi^n = -N(\Psi^n) , \tag{18}$$

where $N'(\Psi^n) = \frac{\partial N}{\partial \Psi^n}(\Psi^n)$

and $$\Delta\Psi^n = \Psi^{n+1} - \Psi^n . \tag{19}$$

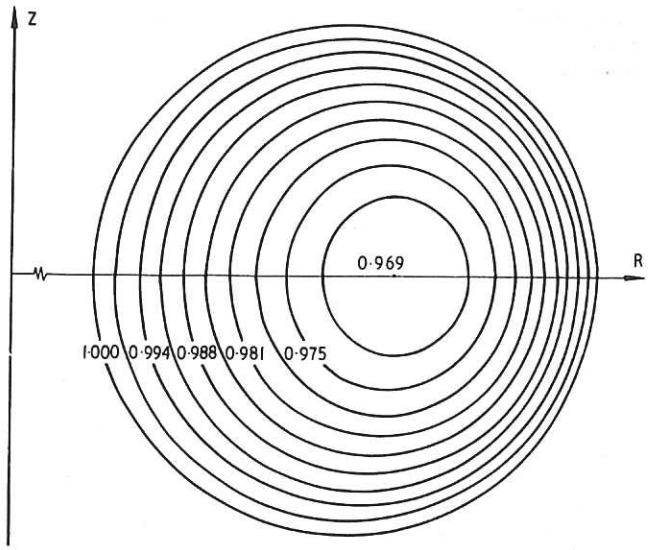

Fig. 2a

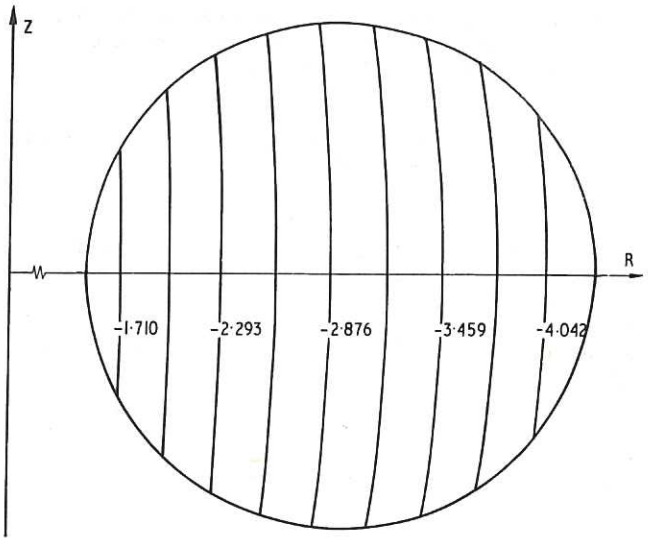

Fig. 2b

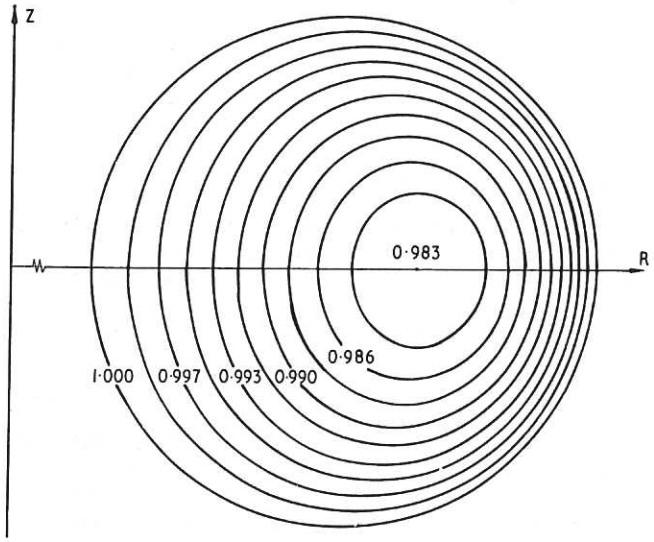

Fig. 3a

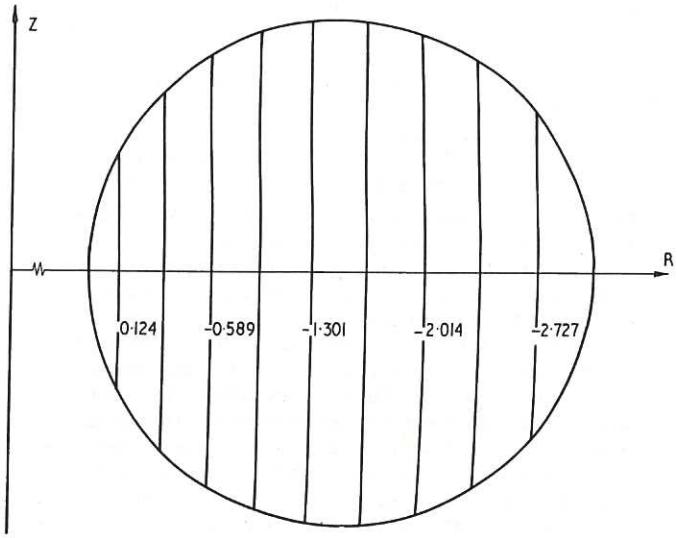

Fig. 3b

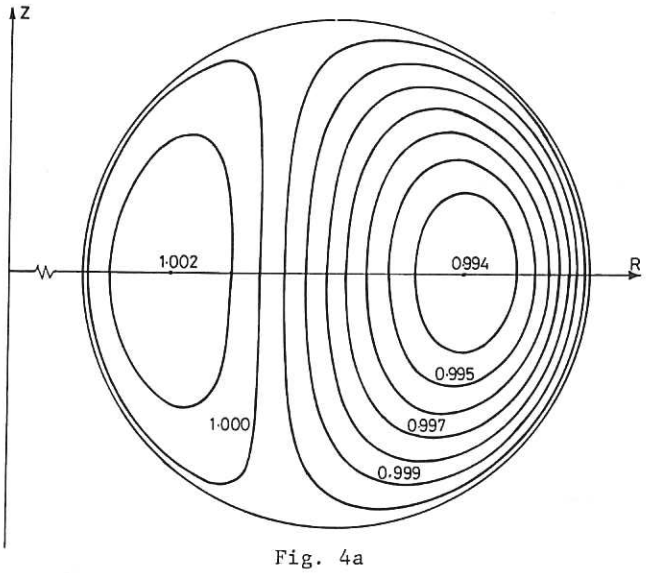

Fig. 4a

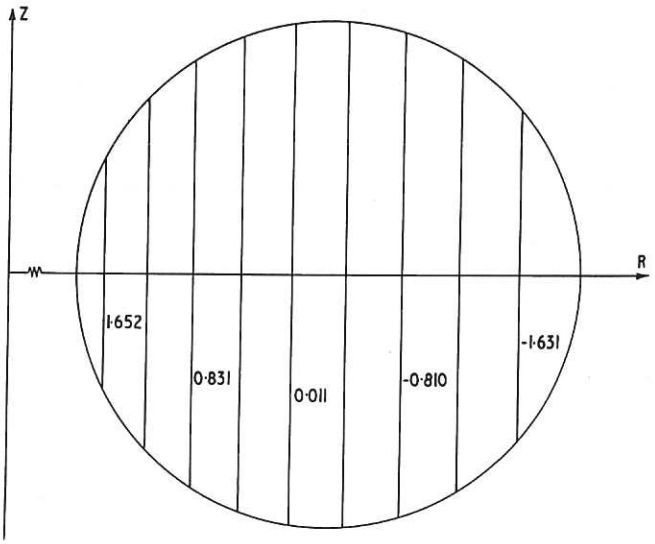

Fig. 4b

Flux Surfaces

Toroidal Current Density Contours

The above figures show flux surfaces and toroidal current density contours (a = 5.0) for the cases d =- 0.4 (Figs. 2a and 2b), d =- 0.7 (Figs. 3a and 3b) and d = - 0.95 (Figs. 4a and 4b).

We take finite differences and have to solve a set of linear equations at each step of the iteration. From Eq. (16) we have

$$N_h'(\Psi^n) = L_h - \frac{\partial f}{\partial \Psi^n}(\Psi^n)\, I\,, \qquad (20)$$

where $N_h'(\Psi^n)$ and L_h are matrices of finite difference coefficients. Hence $N_h'(\Psi^n)$ is the same as L_h except for changes in the diagonal elements of L_h - the derivatives $\partial f/\partial \Psi$ being specified exactly. $N(\Psi^n)$ is just the residual at the n^{th} iteration. The convergence of the method depends on the starting value for the solution and on $\partial f/\partial \Psi$. If $\partial f/\partial \Psi$ makes the matrix N_h' indefinite the system of linear equations cannot be solved by an iterative method.

(A) Circular cross-section

Setting $\epsilon = 0.2$, $a = 5.0$, and considering n, m such that $2 \leq n \leq 5$ and $2 \leq m \leq 5$, the results are presented in Tables 1a and 1b for three values of d, namely $d = -0.4$, -0.7 and -0.9. For $d = -0.4$ a single magnetic axis (a pressure maximum) is found and the toroidal current density is unidirectional. Poloidal-β is of order 1.5 and the results do not depend significantly upon n or m. For $d = -0.7$ a single magnetic axis is again observed, but in this case the toroidal current density reverses. Poloidal-β is of order 3.2 and not significantly affected by the values of n and m. Finally, for $d = -0.9$ two magnetic axes are observed, corresponding to a pressure maximum and a pressure minimum. Since the latter is associated with a negative pressure, the evaluation of β_I is not meaningful in this case. Current reversal is found and again the results are not much affected by n and m. Although β_I has only a weak dependence on m and n, it is possible to discern a pattern in the results for $d = -0.4$ and -0.7. This is brought out clearly in Table 2. We see that for constant m, β_I increases with n. For constant n, β_I decreases as m increases.

To illustrate the general features of the flux-surfaces and toroidal current density contours (for $n = m = 2$, $a = 5.0$, $\epsilon = 0.2$), we give plots of the following cases:

(a) $d = -0.4$ - one magnetic axis, j_φ unidirectional (see Figs. 2a and 2b).

(b) $d = -0.7$ - one magnetic axis, j_φ reversed (see Figs. 3a and 3b).

(c) $d = -0.95$ - two magnetic axes, j_φ reversed (see Figs. 4a and 4b).

Fig. 5 shows a plot of β_I as a function of a and d for $\epsilon = 0.2$, $n = m = 2$. We observe that for the range of parameters considered β_I is essentially independent of a. We have compared the numerical solutions for the cases $d = -0.7$, -0.95 ($a = 5.0$, $\epsilon = 0.2$, $n = m = 2$) with the results obtained from the asymptotic formulae of Eqs. (8) and (9), and find agreement to three decimal places. Although we have considered n and m for which the MHD equilibrium equation is non-linear, as shown earlier, there is an ordering for which the solution is essentially linear, and this is borne out by the computations - there being no evidence of bifurcation. In fact, all the significant features of the theory are supported by the numerical results.

(B) Non-circular cross-section

We now treat the problem of a plasma with a non-circular boundary. Taking the forms given in Eqs. (3) and (4) with $m = n = 2$, we suppose the plasma to have an 'egg-shaped' boundary given by the formula

$$y^2 = (1 - x^2)(1 + \delta^2 - 2\delta x)^{-1}, \qquad (21)$$

and illustrated in Fig. 6. Solving Eq. (14) for the values of a and d taken before, our results are found to be very similar to those for the circular boundary, even when the distortion (δ) of the boundary is significant, $\delta = 0.75$ say. For a given δ a limit on β_I is reached which is again set by the appearance of a second magnetic axis. In Figs. 6a and 6b we give plots

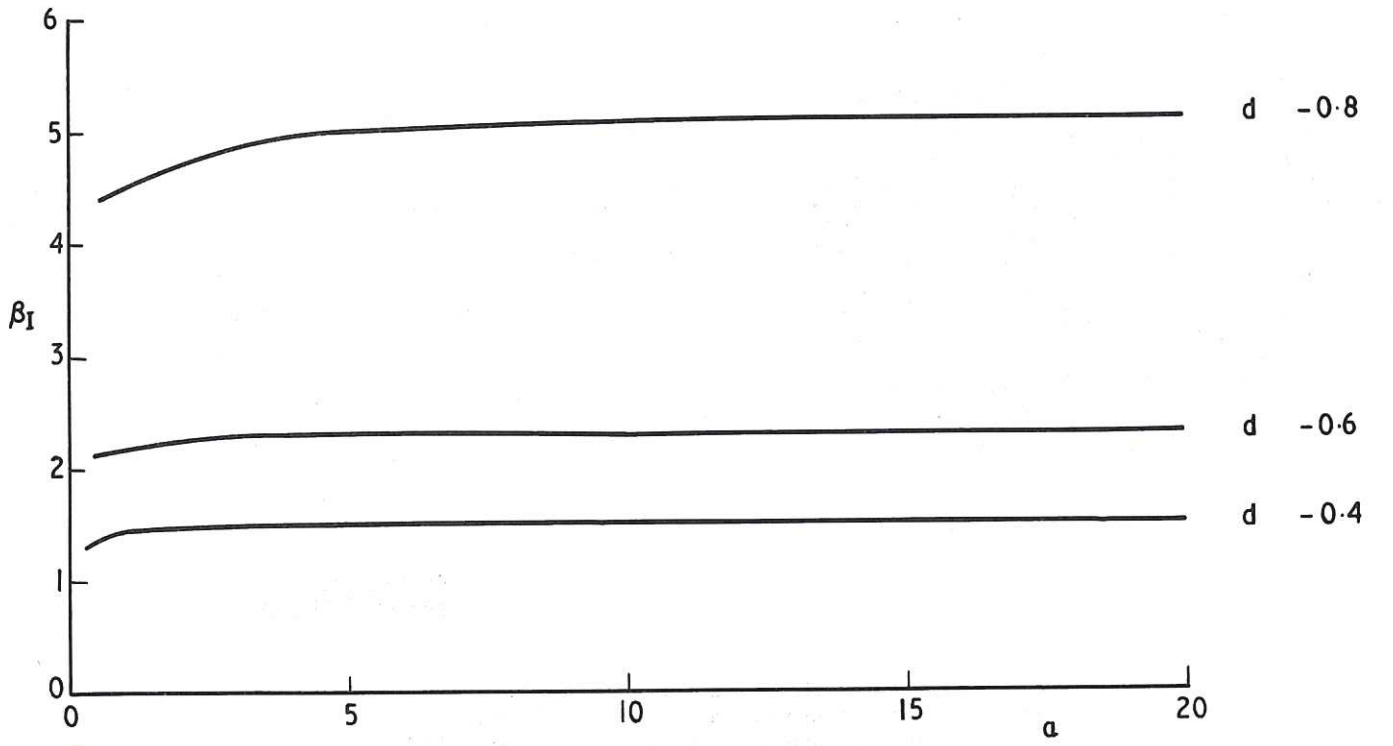

Fig. 5 β_I as a function of a and d.

TABLE 1(a)

a = 5.0 d = - 0.4

(m,n)	Position of pressure maximum	Flux at pressure maximum	β_I
(2,2)	0.2	0.969038	1.4927
(2,3)	0.2	0.970163	1.5032
(2,4)	0.2	0.971217	1.5054
(2,5)	0.25	0.972202	1.5063
(3,2)	0.2	0.968586	1.4923
(3,3)	0.2	0.969746	1.4959
(3,4)	0.2	0.970829	1.4982
(3,5)	0.2	0.971840	1.4993
(4,2)	0.2	0.968131	1.4849
(4,3)	0.2	0.969318	1.4889
(4,4)	0.2	0.970429	1.4914
(4,5)	0.2	0.971466	1.4927
(5,2)	0.2	0.967659	1.4781
(5,3)	0.2	0.968879	1.4823
(5,4)	0.2	0.970019	1.4850
(5,5)	0.2	0.971084	1.4864

a = 5.0 d = - 0.7

(m,n)	Position of pressure maximum	Flux at pressure maximum	β_I
(2,2)	0.3	0.982932	3.1592
(2,3)	0.3	0.983531	3.1958
(2,4)	0.3	0.984090	3.2213
(2,5)	0.35	0.984611	3.2438
(3,2)	0.3	0.982518	3.1349
(3,3)	0.3	0.983148	3.1651
(3,4)	0.3	0.983738	3.1917
(3,5)	0.35	0.984284	3.2154
(4,2)	0.3	0.982086	3.1030
(4,3)	0.3	0.982747	3.1342
(4,4)	0.3	0.983364	3.1622
(4,5)	0.3	0.983940	3.1870
(5,2)	0.3	0.981634	3.0712
(5,3)	0.3	0.982329	3.1035
(5,4)	0.3	0.982973	3.1329
(5,5)	0.3	0.983575	3.1588

TABLE 1(b)

a = 5.0 d = - 0.9

(m,n)	Position of pressure maximum	Flux at pressure maximum	Position of pressure minimum	Flux at pressure minimum
(2,2)	0.45	0.991691	-0.80	1.000749
(2,3)	0.45	0.991937	-0.75	1.000776
(2,4)	0.50	0.992168	-0.75	1.000804
(2,5)	0.50	0.992383	-0.75	1.000830
(3,2)	0.45	0.991481	-0.80	1.000728
(3,3)	0.45	0.991743	-0.80	1.000743
(3,4)	0.45	0.991990	-0.75	1.000781
(3,5)	0.50	0.992218	-0.75	1.000809
(4,2)	0.45	0.991261	-0.80	1.000704
(4,3)	0.45	0.991539	-0.80	1.000732
(4,4)	0.45	0.991798	-0.80	1.000758
(4,5)	0.45	0.992042	-0.75	1.000787
(5,2)	0.45	0.991029	-0.80	1.000677
(5,3)	0.45	0.991323	-0.80	1.000710
(5,4)	0.45	0.991597	-0.80	1.000737
(5,5)	0.45	0.991852	-0.80	1.000763

TABLE 2

Values of β_I

d = - 0.4

m \ n	2	3	4	5
2	1.4927	1.5032	1.5054	1.5063
3	1.4923	1.4959	1.4982	1.4993
4	1.4849	1.4889	1.4914	1.4927
5	1.4781	1.4823	1.4850	1.4864

d = - 0.7

m \ n	2	3	4	5
2	3.1592	3.1958	3.2213	3.2438
3	3.1349	3.1651	3.1917	3.2154
4	3.1030	3.1342	3.1622	3.1870
5	3.0712	3.1035	3.1329	3.1588

TABLE 3

Bifurcation results for the case a = 10.0,
d = - 0.4, m = 2, n = 2, ϵ = 0.2

α	Start	β_I	r_{MA}	Flux at pressure min/max
2000	2.0	2.86	0.2	0.93
2000	1.0		- 0.15	1.01
3500	2.0	2.38	0.2	0.93
3500	1.0		- 0.25	1.01
7500	2.0	2.08	0.2	0.93
7500	1.0		- 0.35	1.01

Note: (1) START is the starting value of the solution taken everywhere except at the wall, where $\Psi_B = 1$.

(2) r_{MA} (position of magnetic axis) has been normalised to a minor radius of 1.

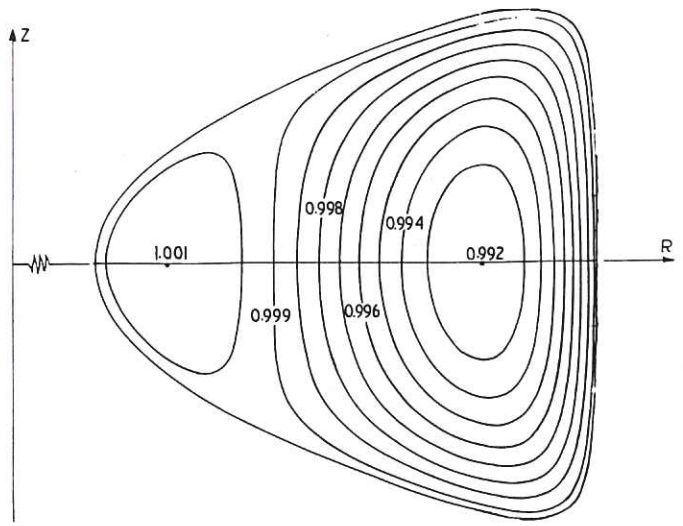

Fig. 6a Flux surfaces for plasma with an "egg-shaped" cross-section (δ = 0.75, a = 5.0, d = - 0.95).

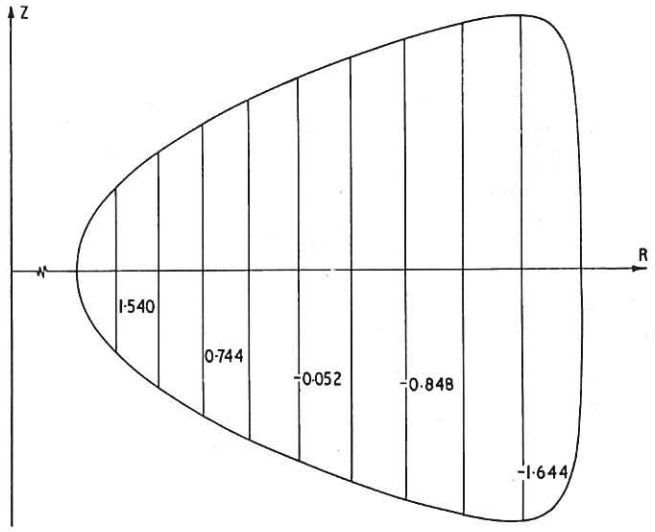

Fig. 6b Toroidal current density contours for δ = 0.75, a = 5.0, d = - 0.95

for the case $\delta = 0.75$, $a = 5.0$, $d = -0.95$. The phenomena of two magnetic axes and current reversal are observed. The curve defined by Eq. (21) touches the sides of a square, and therefore cannot describe cross-sections which are a long way from circular.

3. MODEL II

We now consider a diffuse, circular cross-section model, with $p(\psi)$ and $F(\psi)$ given by

$$p(\psi) = \frac{a\,\psi_B^2}{n\,R_o^4}\left(1 - \left(\frac{\psi}{\psi_B}\right)^n\right)\exp\left(-\frac{1}{\alpha(1-\frac{\psi}{\psi_B})^n}\right), \quad (22)$$

$$\text{and} \quad F(\psi) = \left(C + \frac{2da\,\psi_B^2}{m\,R_o^2}\left(1 - \left(\frac{\psi}{\psi_B}\right)^m\right)\right)^{\frac{1}{2}}, \quad (23)$$

where α is a further free parameter. By choosing α to be sufficiently large we can ensure that for most of the range $0 < \psi < \psi_B$ the pressure has the ψ-dependence adopted in Model I. As ψ approaches ψ_B, however, the exponential dominates. Thus the form for p has the property that $dp/d\psi$, and hence $|\nabla p|$, vanishes at the wall, whilst the toroidal current density is finite. The equation to be solved is non-linear, and takes the form

$$R\frac{\partial}{\partial R}\left(\frac{1}{R}\frac{\partial \Psi}{\partial R}\right) + \frac{\partial^2 \Psi}{\partial Z^2} - a\left[d\Psi^{m-1} + R^2\left(\Psi^{n-1} + \frac{1}{\alpha}\frac{(1-\Psi^n)}{(1-\Psi)^{n+1}}\right)\exp\left(-\frac{1}{\alpha(1-\Psi)^n}\right)\right] = 0, \quad (24)$$

where, as before, $\Psi = \psi/\psi_B$, and $\Psi = 1$ at the boundary.

We examine the case $a = 10.0$, $d = -0.4$, $m = n = 2$ and $\epsilon = 0.2$, and give results for three values of α. For each setting of α two solutions have been found. One shows a single pressure maximum displaced outwards. The other corresponds to an unconfined plasma, the pressure being everywhere negative, and with a pressure minimum displaced inwards. The solution obtained depends on the starting value for Ψ used in the iterative procedure. This is an example of bifurcation, and a similar phenomenon has been observed by Marder and Weitzner[7] in connection with an equilibrium derived from the rigid rotor distribution function. Our results are summarised in Table 3.

In Figs. 7(a), 7(b) and 7(c), we give plots of the poloidal flux, pressure and toroidal current density contours for the confined case corresponding to α = 2,000. The current density contours show the

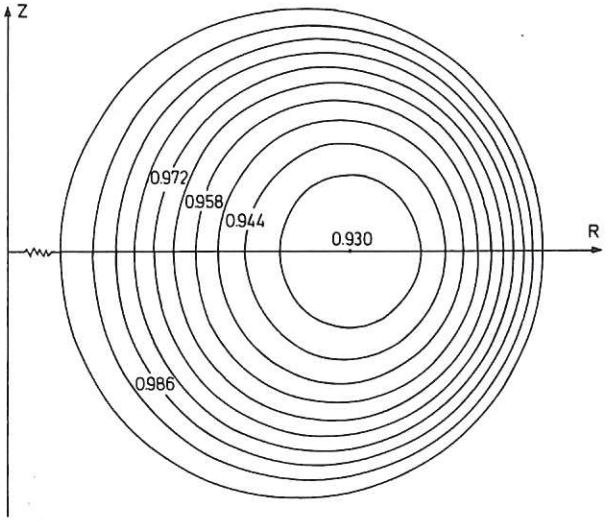

Fig. 7a Flux-surfaces for MODEL II with α = 2,000.

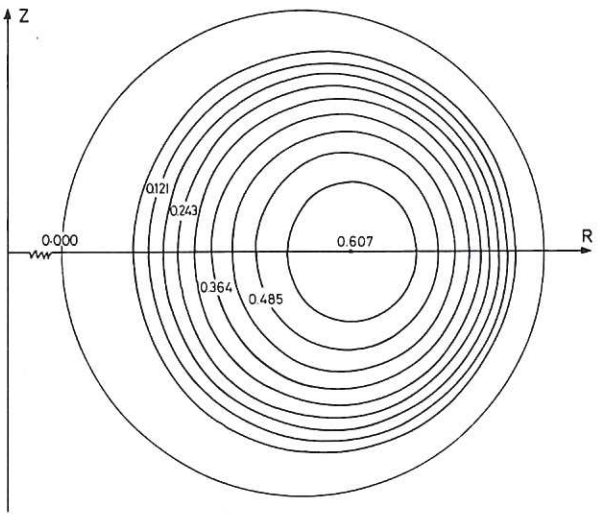

Fig. 7b Pressure contours for MODEL II with α = 2,000.

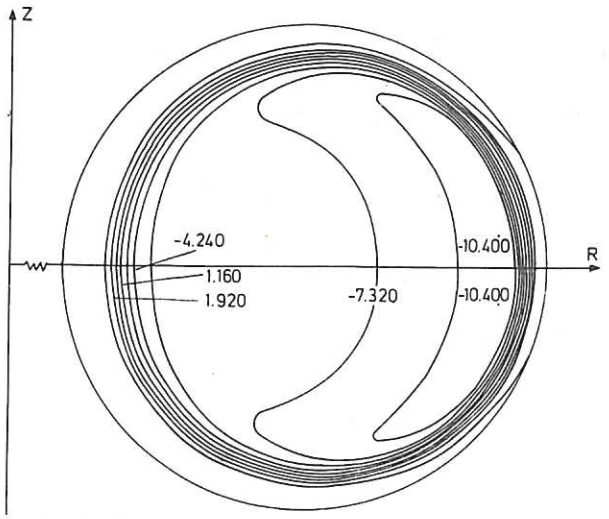

Fig. 7c Toroidal current density contours for MODEL II with α = 2,000.

presence of reversal. As β increases the crescent-shaped current contours move towards the axis of symmetry and eventually join the family of "circular" contours.

Callen and Dory[8] have studied a non-linear equilibrium equation in which p and F are harmonic functions of ψ. Since they found no evidence of bifurcation it is important to confirm our results. Now Marder and Weitzner, in their study of a two-dimensional non-linear equation, demonstrated bifurcation by dropping the Z-dependence, and solving the resulting one-dimensional equation exactly. In the present problem this has not proved possible. We can, however, solve the one-dimensional version of Eq. (24), numerically. Thus, as an independent check, we have used the mutiple-shooting method for two-point boundary value problems as implemented by England[9]. Since England's code requires an initial estimate of the solution, we have used the results pertaining to the plane of symmetry (Z = 0) in the two-dimensional calculation, for this purpose. The shooting method confirms the existence of two distinct solutions for the one-dimensional equation. Each corresponds to a pressure with the same sign as the pressure given by the initial estimate, and hence by the two-dimensional solution.

4. MODEL III

In the models previously described the toroidal current density is non-zero at the boundary. Since this feature is undesirable in a reactor it is of interest to consider a diffuse plasma in which p, $|\nabla p|$ and j_φ, all vanish at the boundary $\psi = \psi_B$. For such a mode, Eq. (2) has the trivial solution $\psi = \psi_B$, and this suggests the existence of eigenfunctions. By taking the cross-section to be square we can develop asymptotic analysis, thus illustrating the essential physical features. We choose the following forms for p and F:

$$p = \frac{a}{2R_o^2 S^2}(\psi_B - \psi)^2 \qquad (25)$$

and

$$F = \frac{1}{S}\left[C + 2b\left(\psi_B\psi - \frac{\psi^2}{2}\right)\right]^{\frac{1}{2}}, \qquad (26)$$

where a, b and C are free parameters, and 2S is the side of the square cross-section. These forms ensure that the required boundary properties are satisfied, and that the pressure is positive everywhere.

(i) Asymptotic Analysis

We introduce dimensionless rectangular coordinates (x, y) based on the centre O, of the minor cross-section (see Fig. 8). The

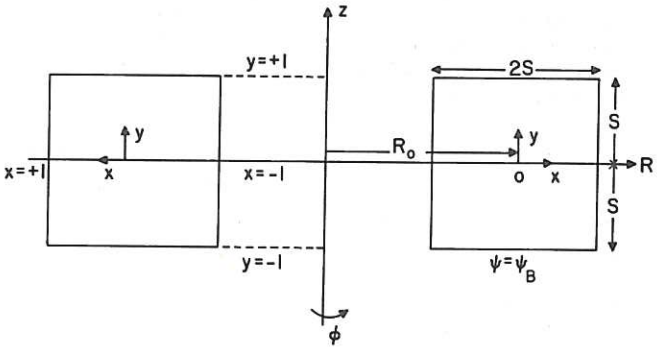

Fig. 8 Coordinate systems for a square cross-section plasma.

mathematical transformations are straightforward and Eq. (2) can be written as

$$\frac{\partial^2\Psi}{\partial x^2} + \frac{\partial^2\Psi}{\partial y^2} - \frac{\epsilon}{1+\epsilon x}\frac{\partial\Psi}{\partial x} + (1-\Psi)(b - a(1+\epsilon x)^2) = 0, \qquad (27)$$

where $\Psi = \psi/\psi_B$ and $\Psi = 1$ at the boundary. Choosing the dimensionless parameters a and b to have the ordering $a \sim b \sim \epsilon^{-1}$, where $a - b \sim 1$, Eq. (27) can now be solved by expanding Ψ in the form

$$\Psi = 1 + \Psi_1 + \ldots . \qquad (28)$$

It follows that Eq. (27) becomes[10]

$$\frac{\partial^2\Psi_1}{\partial x^2} + \frac{\partial^2\Psi_1}{\partial y^2} + \Psi_1(a - b + 2a\epsilon x) = 0 , \qquad (29)$$

where the boundary conditions are periodic, namely $\Psi_1 = 0$ at $x = \pm 1$ and $y = \pm 1$.

Assuming Ψ_1 to have the form

$$\Psi_1 = \cos\left(\frac{\pi}{2}y\right)E(x) , \qquad (30)$$

then E(x) satisfies the equation

$$\frac{d^2E}{dx^2} + B^3(\Lambda + x)E = 0 , \qquad (31)$$

where $B = (2a\epsilon)^{\frac{1}{3}}$ and $\Lambda = [a - b - (\pi/2)^2]B^{-3}$. Defining the new independent variable $\rho = B(\Lambda + x)$, Eq. (31) can be written as

$$\frac{d^2E}{d\rho^2} + \rho E = 0 , \qquad (32)$$

which is Airy's equation. The solution of Eq. (32) can be written in the form

$$E = P\,Ai(-\rho) + Q\,Bi(-\rho) , \qquad (33)$$

where P and Q are arbitrary coefficients. Applying the boundary condition $E = 0$ at $x = -1$, Eq. (33) becomes

$$E = P\left\{Ai(-\rho) - \frac{Ai(-B(\Lambda-1))}{Bi(-B(\Lambda-1))}Bi(-\rho)\right\}. \qquad (34)$$

For E to vanish at $x = +1$, B and Λ must

be related through the expression

$$\frac{Ai(-X)}{Bi(-X)} = \frac{Ai(-X-2B)}{Bi(-X-2B)} , \qquad (35)$$

where $X = B(\Lambda - 1)$. Thus for a physical solution to exist, the parameters a and b are related through Eq. (35). The eigenfunction nature of the problem is brought out more clearly by writing (31) as

$$\frac{d^2E}{dx^2} + B^2(X + B + Bx) = 0 . \qquad (36)$$

Thus if we select a value for X, solutions arise for all values of B given by Eq. (35). The Airy functions have been tabulated by Abramowitz and Stegun[11] and we give a plot of their ratio Ai(- X)/Bi(- X), in Fig. 9. We observe that

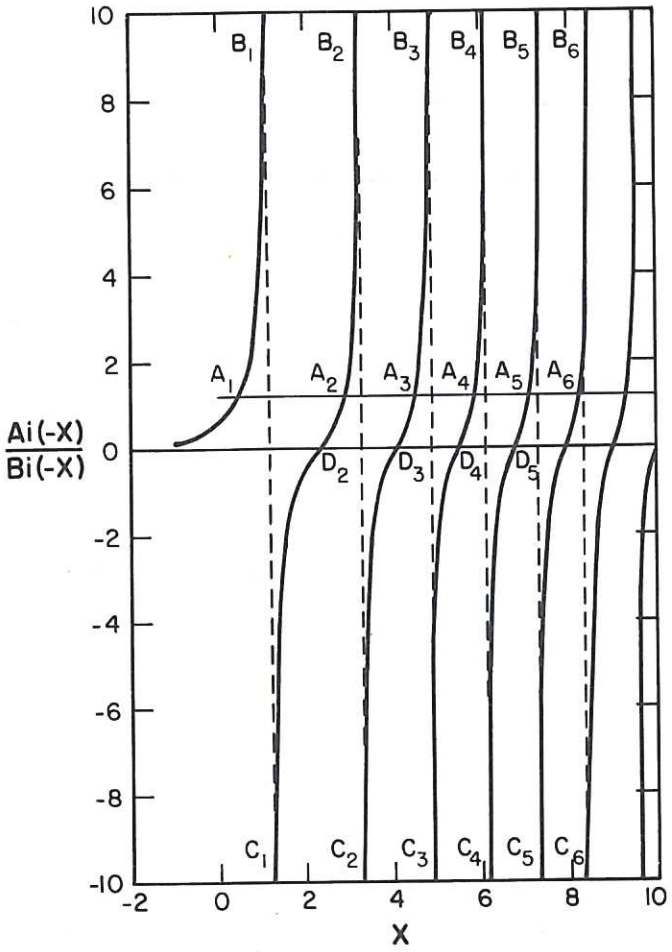

Fig. 9 Plot of Ai(- X)/Bi(- X) against X.

the various branches of this function approach the vertical lines B_1C_1, B_2C_2, B_3C_3... asymptotically. For X corresponding to the point A_2, Eq. (35) is satisfied for values of B given by $2B = A_1A_2$, A_2A_3, A_2A_4, ... For each value of B in this series there is a corresponding value of Λ. Since B is positive, choosing $X \geq 0$ implies $\Lambda \geq 1$, whereas for $X < 0$, we must have $\Lambda < 1$. Thus the procedure is to select a value for X, determine B (and hence Λ) through Eq. (35), and then to plot E(x) and $\Psi_1(x, y)$. This process is then repeated for all values of X.

Having solved the equilibrium equation, it is of considerable interest to evaluate the toroidal current density, β and β_I. It is straightforward to show that the dimensionless current density is given by

$$\frac{s^2R_o}{\psi_B} j_\varphi = \left[\left(\frac{\pi}{2}\right)^2 + B^3(\Lambda + x)\right] \Psi_1 . \qquad (37)$$

To leading-order, the total - β is given by

$$\beta = \frac{a\psi_B^2}{s^2R_o^2 B_{\varphi o}^2} \Psi_{1ma}^2 , \qquad (38)$$

where Ψ_{1ma} denotes the first-order poloidal-flux at the magnetic axis. Using Eq. (26), the zero-order toroidal field $B_{\varphi o}$, can be written as

$$B_{\varphi o}^2 = \frac{1}{s^2R_o^2}(C + b\psi_B^2) . \qquad (39)$$

It follows that

$$\beta = \frac{a\Psi_{1ma}^2}{b + C\psi_B^{-2}} . \qquad (40)$$

Recalling that $a \sim b \sim \epsilon^{-1}$, we choose C to be negative, of order $\psi_B^2 \epsilon^{-1}$, and such that $b + C\psi_B^{-2} \sim 1$. This ordering ensures that $\beta \sim \epsilon$. It should be noted that to assume any other order for C would contravene the basic tenet for Tokamak, namely that $\frac{s}{R_o}\frac{B_\varphi}{B_y} \sim 1$.

To obtain a number for β it is necessary to specify a value for C, and also to choose a suitable normalization for Ψ_1. Both these features, however, are avoided in the evaluation of poloidal-β, since this quantity is independent of C and P. The poloidal -β can be expressed in the form

$$\beta_I = \frac{\frac{\pi^3}{8\epsilon}\int_X^{X+2B}\left(Bi(-X)\,Ai(-\rho) - Ai(-X)\,Bi(-\rho)\right)^2 d\rho}{\left[\int_X^{X+2B}\left(Bi(-X)Ai(-\rho)-Ai(-X)Bi(-\rho)\right)\left(\rho + (\tfrac{\pi}{2})^2 B^{-2}\right)d\rho\right]^2} . \qquad (41)$$

We now give some typical results of the asymptotic analysis. Referring to Fig. 9, we take the point A_1 to lie at the value X = - 1.8, and then A_2 corresponds to B = 2.07 and Λ = 0.13. Setting the amplitude P, equal to unity, the solution E(x) is shown as curve I in Fig. 10. The poloidal-flux surfaces Ψ_1 are plotted in Fig. 12. This example shows the presence of one outwardly displaced mag-

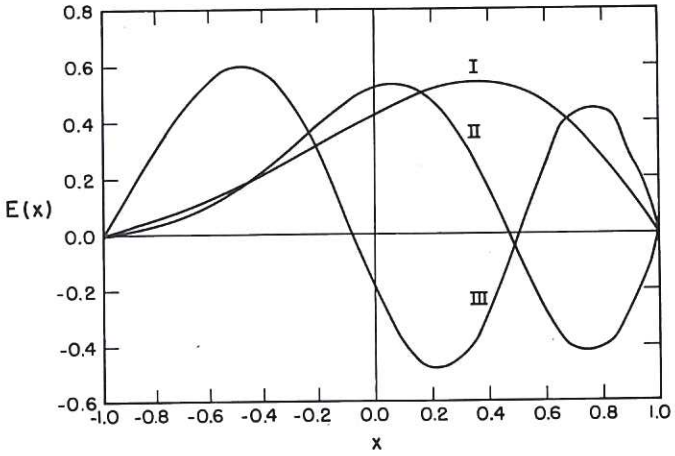

Fig. 10 Plot of E(x) for one (curve I), two (curve II), and three (curve III) magnetic axes.

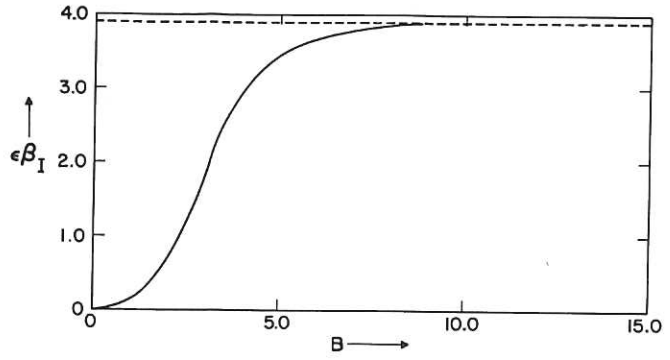

Fig. 11 Plot of $\epsilon\beta_I$ versus B (= $(2a\epsilon)^{\frac{1}{3}}$). This parameter is related to the displacement of the magnetic axis [12].

netic axis corresponding to a pressure maximum, where $\beta_I = 0.81\epsilon^{-1}$. To cover all values of X we start with the line A_1A_2 at $-\infty$ D_2 and take it up to B_1B_2, and then from C_1C_2 to B_2B_3, and so on. We determine B and Λ for each setting of X, and hence evaluate the corresponding β_I. A plot of $\epsilon\beta_I$ against B is shown in Fig. 11. We observe that β_I approaches the limit 3.88 ϵ^{-1} as B increases indefinitely, a result found previously by Haas and Thomas [12].

We now consider A_1 to lie at the value X = - 2.5. For the point A_3 this gives B = 3.29 and Λ = 0.24. The appropriate E(x) is plotted in Fig. 10 (curve II), and poloidal flux-surfaces are sbown in Fig. 13. This example demonstrates the existence of two pressure maxima separated by a pressure minimum with p = 0. To cover all X, we start with the line A_1A_3 at $-\infty$ D_3 and raise it to B_1B_3, and then from C_1C_3 to B_2B_4 and so on.

Lastly, we consider A_1 to lie at the value X = 0.1. For the point A_4 this gives B = 2.83 and Λ = 1.04. The solution is plotted in Fig. 10 (curve III), and the flux-surfaces are displayed in Fig. 14. Three pressure maxima are observed.

The curves for E in Fig. 10 show character-

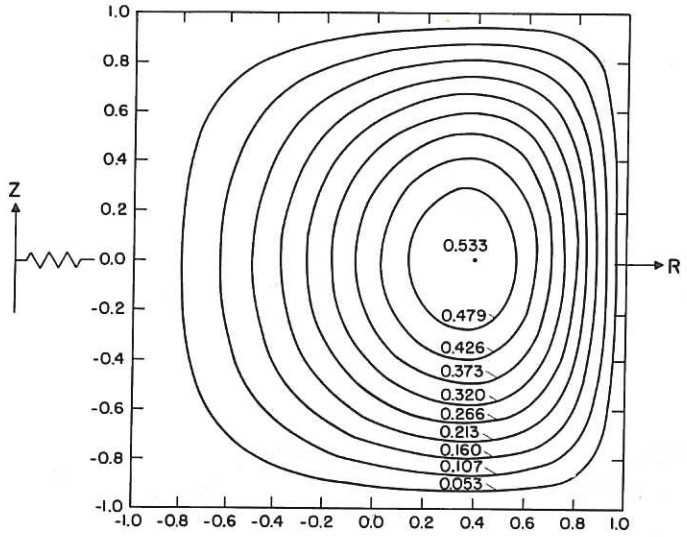

Fig. 12

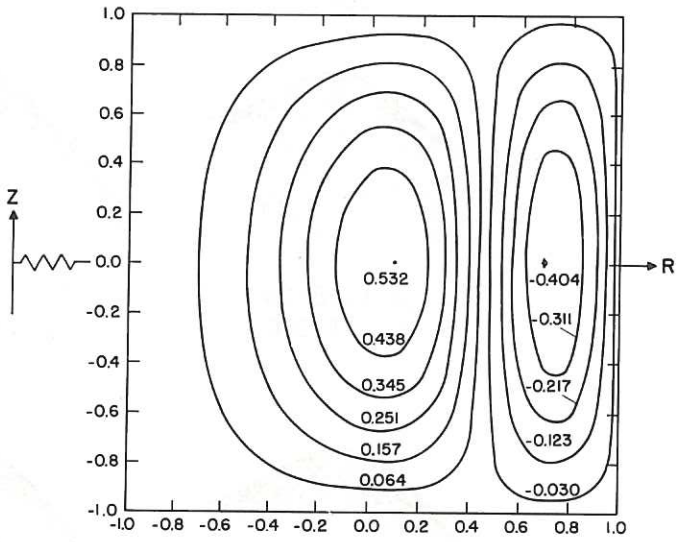

Fig. 13

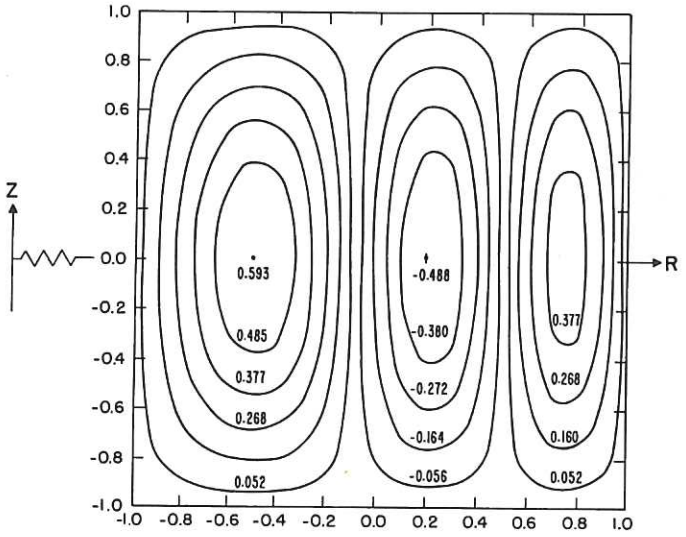

Fig. 14

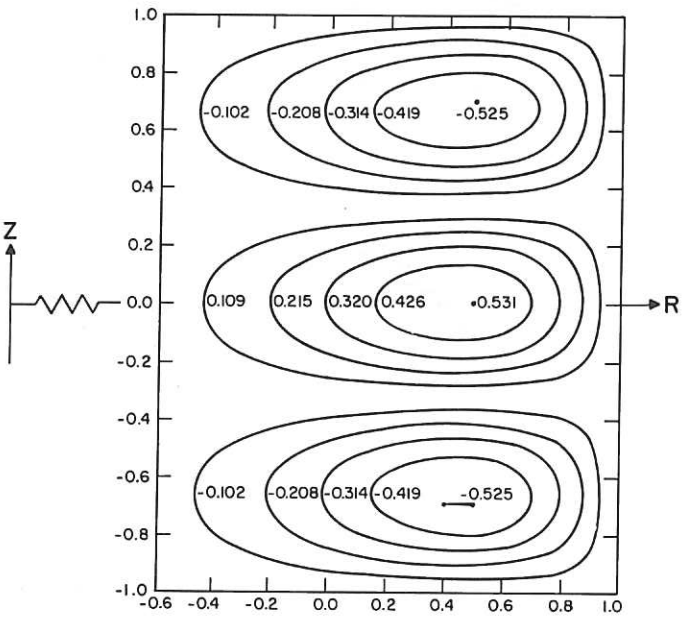

Fig. 15

Flux surfaces

The figures show flux surfaces corresponding to the "fundamental" (Fig. 12) and first and second "harmonics" (Figs. 13 and 14) respectively. Fig. 15 shows flux surfaces corresponding to $\Psi_1 = \cos\left(\frac{3\pi y}{2}\right)E_1(x)$

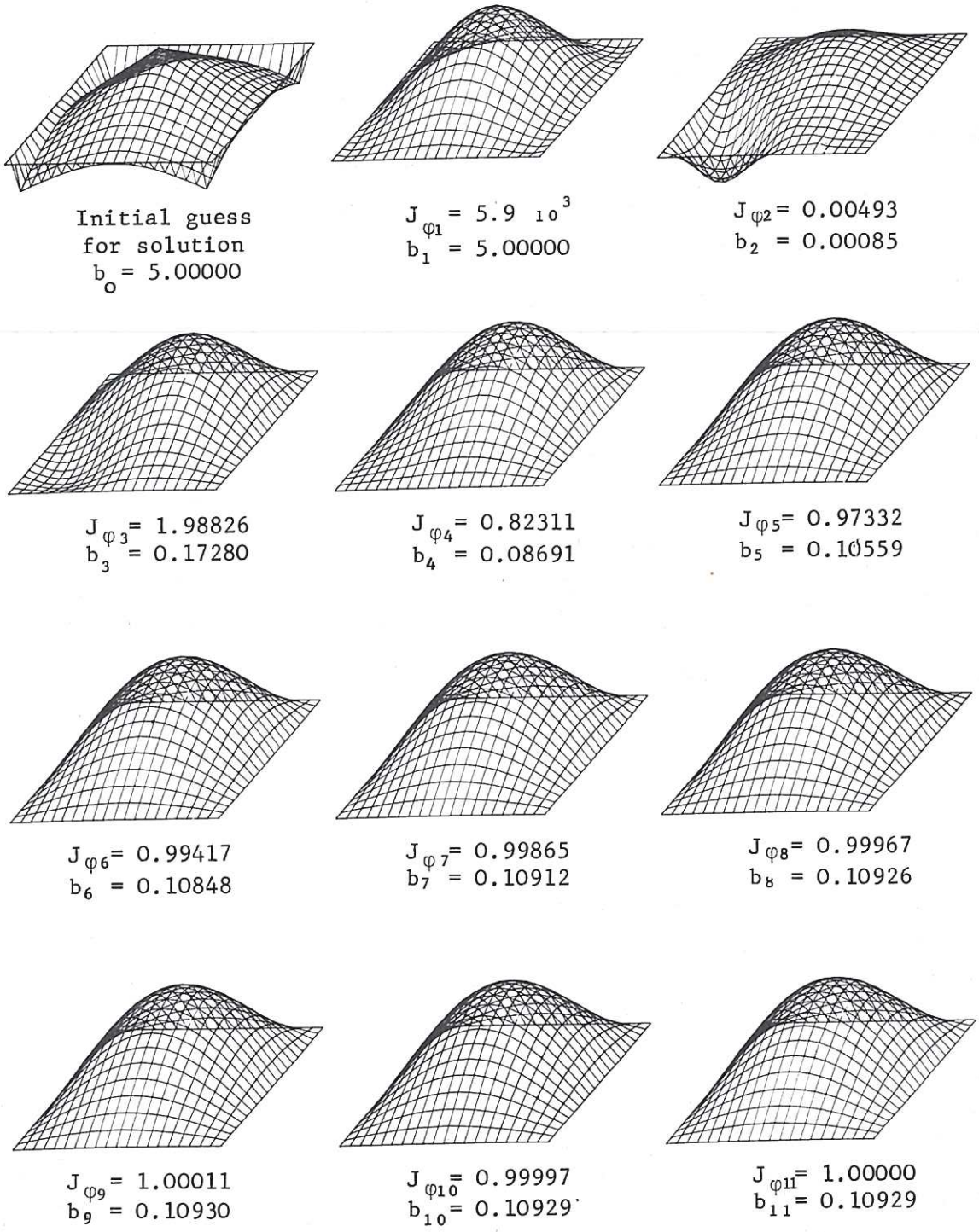

Fig. 16 Isometric views of the solution for the case $b = 0.109$, $a = -20$ and $J_\varphi = 1.0$. The figures illustrate the iterative development of the flux-surfaces, values of the toroidal current density, and the adjustable parameter b.

istics resembling the fundamental and harmonics of an eigenvalue problem. Ignoring the limitations of the ordering, these results indicate that for our particular model the number of magnetic axes is unlimited. However, the present calculation is not a real eigenvalue problem since we cannot identify a true eigenvalue, each "eigenfunction" corresponding to a continuous range of the parameters B and Λ. We observe from Eq. (37) that for $X > 0$ (that is, $\Lambda > 1$), the sign of j_φ is determined by the sign of Ψ_1. Thus the number of current reversals will depend on the number of sign changes in E. It follows that for $X > 0$ the single magnetic axis case has a unidirectional current, whereas the double magnetic axis case has one current reversal. Similarly, the triple magnetic axis case has two current reversals. In view of the reversals in j_φ, these multi-pressure maxima equilibria are unlikely to be of practical interest for Tokamak. For $X < 0$ the number of current reversals depend on the details of the particular case under consideration. Of course we can consider solutions of the type

$$\Psi_1 = \cos\left((2n+1)\frac{\pi y}{2}\right) E_n(x) \ , \qquad (42)$$

and these will also show a multiplicity of axes - an example is given in Fig. 15.

(ii) Computations

Using the forms given in Eqs. (25) and (26), and normalising R and Z with respect to the minor radius, the equation to be solved is

$$R\frac{\partial}{\partial R}\left(\frac{1}{R}\frac{\partial \Psi}{\partial R}\right) + \frac{\partial^2 \Psi}{\partial Z^2} + (1-\Psi)(b - a\epsilon^2 R^2) = 0 \ , \qquad (43)$$

with $\Psi = 1$ on the boundary. As before, we consider the plasma to have a square cross-section. Following the asymptotic analysis, we expect Eq. (43) to have a non-trivial solution if a and b are appropriately related. Using Newton's method, the iteration always converges to the trivial solution $\Psi = 1$, for any starting value of Ψ. Thus it is necessary to devise a different procedure.

Symbolically, we can write Eq. (43) in the form

$$L\,\Psi = f(\Psi, R) \ . \qquad (44)$$

Lackner,[13] Fisher,[14] Marder and Weitzner[7] have shown that the most straightforward iterative scheme for Eq. (44) namely,

$$L\,\Psi^{n+1} = f(\Psi^n, R) \ , \qquad (45)$$

has only a limited range of convergence. For an equation such as (43), the iterations will always converge to the trivial solution. To overcome this difficulty Feneberg and Lackner[15] adopt the more general iterative scheme

$$L\,\Psi^{n+1} = f_n(\Psi^n, R) \ . \qquad (46)$$

The essence of this method is to vary one or more parameters in $f(\Psi, R)$ such that an equal number of physical quantities are kept constant. The latter quantities are chosen so as to avoid the trivial solution.

In the present computations we have kept the total toroidal current ($\mathcal{I}$) constant. Introducing the dimensionless toroidal current, $J_\varphi (= \mathcal{I} R_0/\Psi_B)$, and using Eq. (43), we can express this quantity as

$$J_\varphi = \int \frac{(1-\Psi)}{R}(b - a\epsilon^2 R^2)\,dR\,dZ \ , \qquad (47)$$

where the integral is over the plasma cross-section. It is clear that by maintaining J_φ constant throughout the calculation, the trivial solution $\Psi = 1$ must be avoided, since the latter corresponds to $J_\varphi = 0$. In practice we have used Eq. (47) in the form

$$J_\varphi = b\int \frac{(1-\Psi)}{R}(1 - a_1\epsilon^2 R^2)\,dR\,dZ \ , \qquad (48)$$

where $a_1 = a/b$. With J_φ thus defined we can now implement the iterative scheme of Eq. (46).

The steps are as follows:

(a) Specify J_φ and a_1, and make suitable "guesses" at b^0 and Ψ^0 (the starting solution).

(b) Calculate Ψ^1 from Eq. (46) and $J_\varphi{}^1$ from Eq. (48).

(c) If $J_\varphi{}^1 \neq J_\varphi$ then set $b^1 = b^0 J_\varphi / J_\varphi{}^1$. This scales the toroidal current so that $J_\varphi{}^1 = J_\varphi$. The quantity b_0 is then replaced by b_1.

(d) The procedure of (b) and (c) is repeated until some predefined convergence criterion is satisfied. In the calculations reported here, we took $|J_\varphi{}^{n+1} - J_\varphi{}^n| \leq 10^{-4} J_\varphi$, as our criterion.

A typical example of this method of solution is shown in Fig. 16. The corresponding plots of poloidal flux and current density contours are shown in Figs. 17(a) and 17(b).

We now compare the numerical solution with that obtained from the asymptotic analysis for the single pressure-maximum case. For simplicity, we only present results for the plane of symmetry ($Z = 0$). In Fig. 18 we plot the numerical solution pertaining to the case $\epsilon = 0$, $J_\varphi = 5.0$, $b = 4.071$ and $a = -0.814$, for which $\beta_I = 0.82$ and the pressure maximum is at 0.1. The asymptotic analysis, corresponding to these values for a and b ($B = 1.175$ and $\Lambda = 1.485$), leads to the values indicated by the circled points, with $\beta_I = 0.80$ and the pressure maximum at 0.1. The two sets of results are seen to be in good agreement.

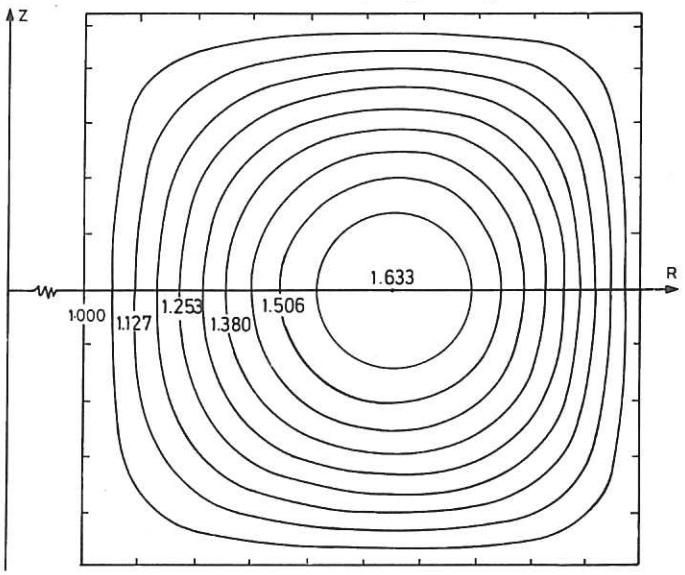

Fig. 17a Flux-surfaces corresponding to the case $b = 0.109$, $a = -20$ and $J_\varphi = 1.0$.

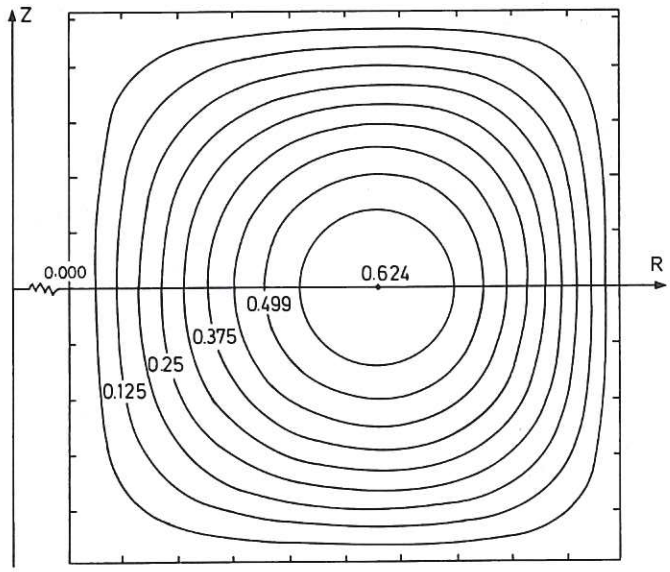

Fig. 17b Toroidal current density contours for the case b = 0.109, a = - 20 and J_φ = 1.0.

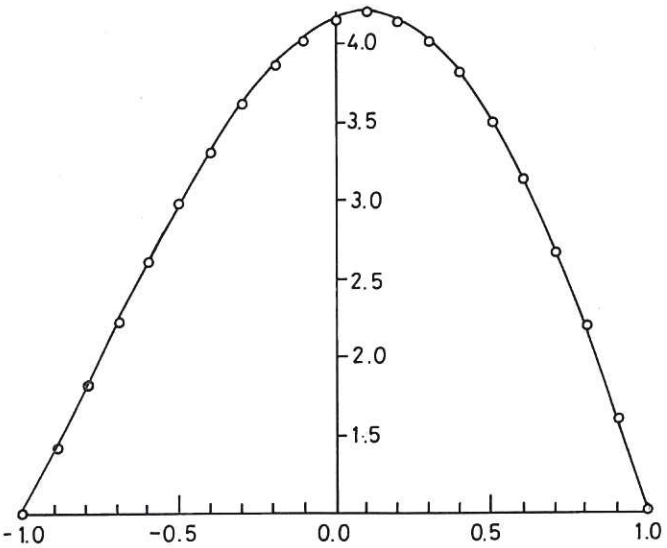

Fig. 18 Comparison of asymptotic analysis and numerical results for the case b = 4.071, a = - 0.814, and J_φ = 5.0 (B = 1.175, Λ = 1.485)

5. MODEL IV

In this model, we consider the plasma to be surrounded by a vacuum region, which is, in turn, enclosed by a perfect conductor. Defining ψ at the plasma vacuum interface to be ψ_B, and ψ at the conducting wall to be ψ_W, we choose the forms

$$p = \frac{a\psi_B^2}{2R_o^4}\left(1 - \frac{\psi}{\psi_B}\right)^2 \qquad (49)$$

and

$$F = [C - 2dR_o^2 p(\psi)]^{\frac{1}{2}} , \qquad (50)$$

for the plasma region, $\psi \geq \psi_B$, and

$$p = 0 , \qquad (51)$$

and

$$F^2 = C , \qquad (52)$$

for the vacuum region, $\psi_B > \psi > \psi_W$. Thus we have to solve the equations

$$R\frac{\partial}{\partial R}\left(\frac{1}{R}\frac{\partial \Psi}{\partial R}\right) + \frac{\partial^2 \Psi}{\partial Z^2} = a(R^2 - d)(1 - \Psi) \qquad (53)$$

for $\Psi \geq 1$, and

$$R\frac{\partial}{\partial R}\left(\frac{1}{R}\frac{\partial \Psi}{\partial R}\right) + \frac{\partial^2 \Psi}{\partial Z^2} = 0 , \qquad (54)$$

for $1 > \Psi > \Psi_W$, subject to the boundary conditions that the normal derivative of Ψ at the interface is continuous, that is

$$\frac{\partial \Psi}{\partial n}_{vac} = \frac{\partial \Psi}{\partial n}_{plasma} \qquad (55)$$

As before, Eqs. (53) and (54) are normalised to the major radius.

Numerically we treat the equilibrium as described by a single equation for which the right-hand side has a discrete change in form at $\Psi = 1$. Since the MHD equation can be written in the form

$$\nabla.\left(\frac{\nabla \Psi}{R^2}\right) = \frac{1}{R}\frac{R_o^3}{\psi_B} j_\varphi , \qquad (56)$$

the boundary condition of Eq. (55) may be derived directly using Gauss's theorem. As the equation to be solved admits the trivial solution $\Psi = \Psi_W$, we must use the procedure introduced for the previous model in order to obtain a physically significant solution. As for the previous model, the forms for p and F ensure that the poloidal current density vanishes at the plasma boundary.

We present results for systems maintained in equilibrium by a "D-shaped" conductor with equation

$$\mu R^2 Z^2 + (R^2 - 1)^2 = \Gamma , \qquad (57)$$

where R and Z are normalised with respect to the major radius, and μ and Γ are free parameters. We give results for μ = 2.747 and Γ = 0.721. For our first example we choose d = C = 0 (no toroidal field), J_φ = 5.0 and Ψ_W = 0.5. The corresponding value for the poloidal-β is β_I = 1.0. Figs. 19a and 19b show the associated flux-surfaces and dimensionless toroidal current density contours ($j_\varphi R_o^3/\psi_B$), respectively. For our second example we take d = 0.5, J_φ = 5.0 and Ψ_W = 0.9, and give results for different values of C. The value for poloidal β is β_I = 2.1. Figs. 20a and 20b show the flux-surfaces and dimensionless toroidal current density contours for this case. Fig. 20b illustrates the phenomenon of current reversal. The safety-factor q, which we define to be

$$q = \frac{1}{2\pi}\oint \frac{B_\varphi}{RB_{pol}}\, d\ell , \qquad (58)$$

has the value 0.3 at the magnetic axis and 1.8 at the plasma boundary for the value C = 36. Since the toroidal field is low at the magnetic axis, we expect the $|B|$ surfaces to be closed in this vicinity, and this feature is demonstrated in Fig. 21a. As C is increased (that is, the toroidal field) the family of closed $|B|$ surfaces disappears. This is shown in Figs. 21b and 21c for C = 72 and C = 100, respectively.

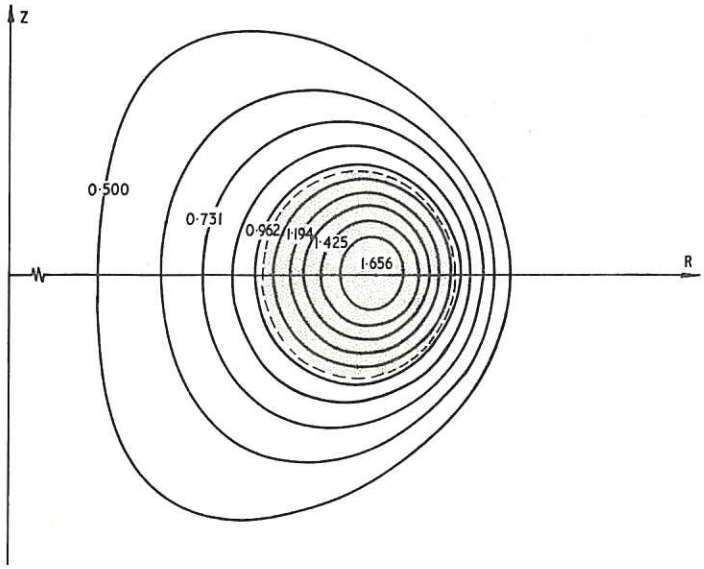

Fig. 19a

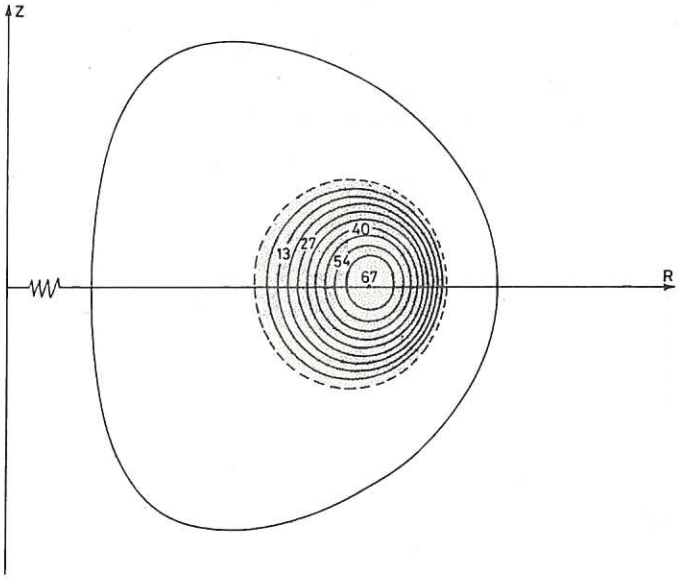

Fig. 19b

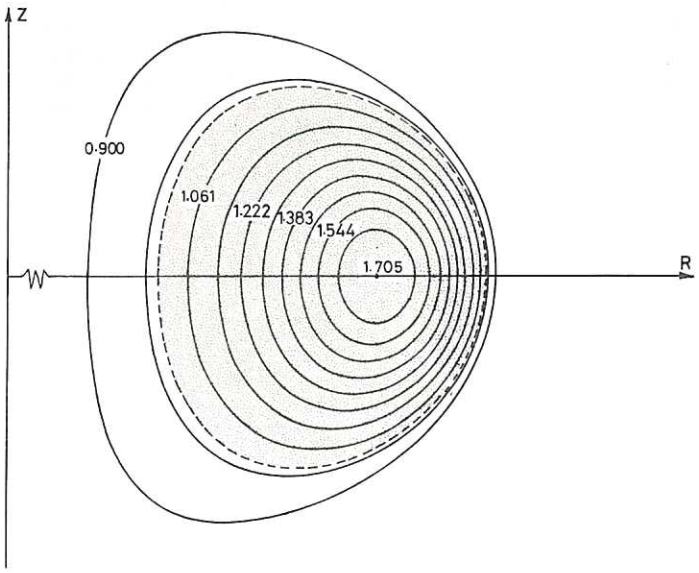

Fig. 20a

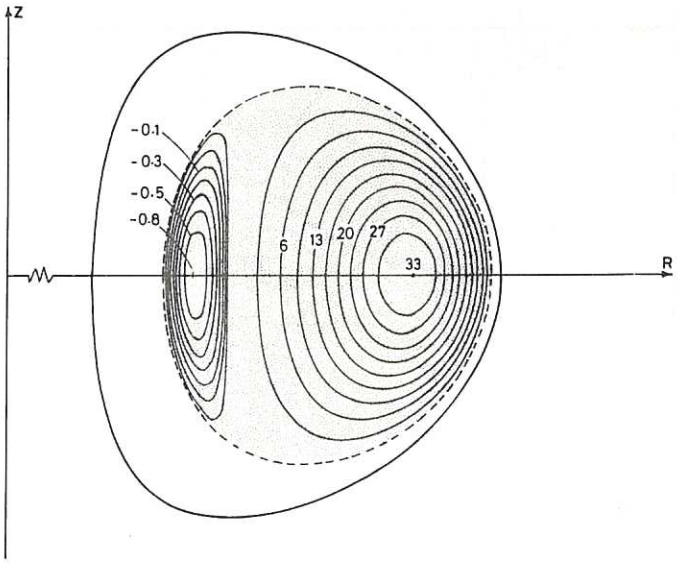

Fig. 20b

Flux Surfaces

Toroidal Current Density Contours

The figures show flux surfaces and toroidal current density contours for the cases d = C = 0 and $\Psi_w = 0.5$ (Figs. 19a, 19b) and d = 0.5, C = 0 and $\Psi_w = 0.9$ (Figs. 20a, 20b). In each figure the dotted curve represents the plasma boundary.

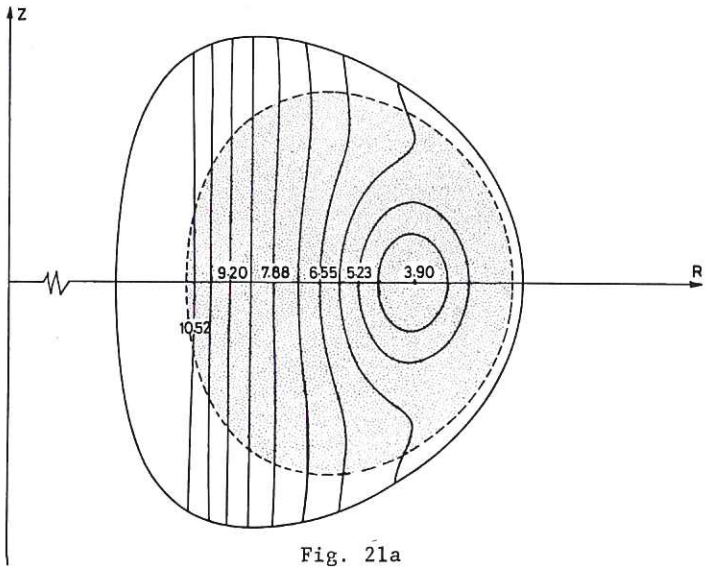

Fig. 21a

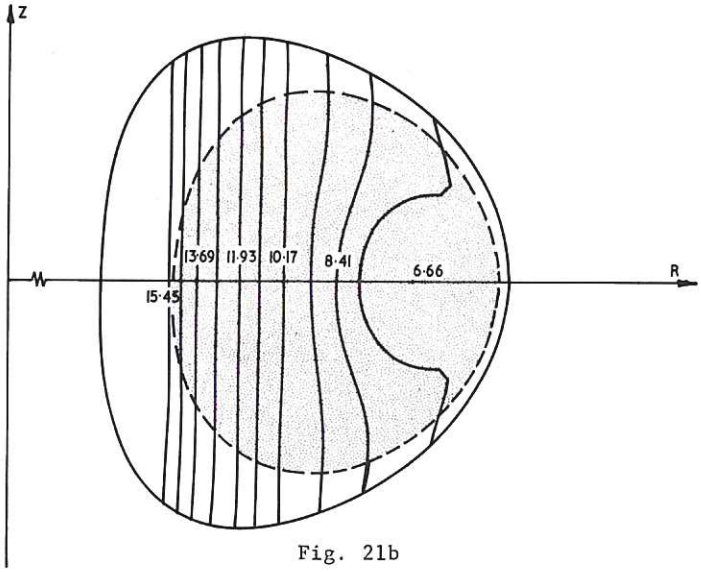

Fig. 21b

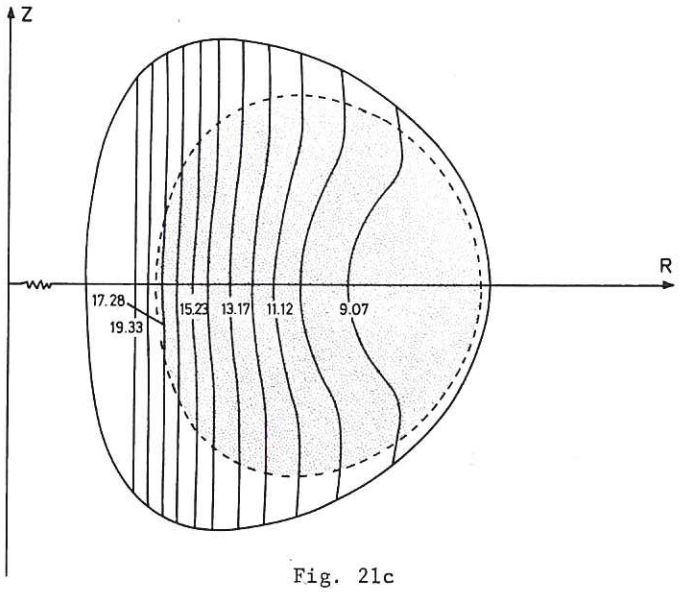

Fig. 21c

Dimensionless $|B|$ surfaces $\left(\frac{|B|R_o^2}{\psi_B}\right)$

The figures show $|B|$ surfaces ($d = 0.5$, $\Psi_w = 0.9$) for the cases $C = 36$ with $q = 0.3$ at magnetic axis and $q = 1.8$ at plasma boundary (Fig. 21a), $C = 72$ with $q = 0.5$ at magnetic axis and $q = 2.6$ at plasma boundary (Fig. 21b), and $C = 100$ with $q = 0.6$ at magnetic axis and $q = 3.0$ at plasma boundary (Fig. 21c).

Acknowledgments

The authors are grateful to Prof K.W. Morton of the University of Reading, and to Drs v. Hagenow and Lackner of the Max-Planck-Institut für Plasmaphysik, Garching, for stimulating discussions.

REFERENCES

1. Laing, E.W., Roberts, S.J. and Whipple, R.T.P., J. Nucl. Energy, Part C: Plasma Physics 1, 49 (1959).

2. Thomas, C.Ll., Culham Report CLM-P 339 (1973).

3. Grad, H. and Hogan, J., Phys. Rev. Lett. 24, 1337 (1970).

4. Gourdon, C. and Touche, J., EUR-CEA-FC 634 (1972).

5. Adam, J.C. and Mercier, C., in Plasma Physics and Controlled Nuclear Fusion Research, (International Atomic Energy Agency, Vienna, 1969), Vol. I, 199.

6. Laval, G., Maschke, E.K., Pellat, R. and Rosenbluth, M.N., International Centre for Theoretical Physics, Report IC/70/35 (1970).

7. Marder, B. and Weitzner, H., Plasma Phys. 12, 435 (1970).

8. Callen, J.D. and Dory, R.A., Phys. Fluids 15, No. 8, 1523 (1972).

9. England, R., Culham Report CLM-PDN 3/73 (1973).

10. Strauss, H.R., Phys. Rev. Lett. 26, 616 (1971).

11. Abramowitz, M. and Stegun, I.A., Dover Publication, Inc. New York (1965).

12. Haas, F.A. and Thomas, C.Ll., Phys. Fluids 16, No. 1, 152. (1973).

13. Lackner, K., J. Geophys. Res., 75, 16 (1970).

14. Fisher, S., Phys. Fluids 14, 962 (1971).

15. Feneberg, W. and Lackner, K., Nuclear Fusion 13, 549 (1973).

HER MAJESTY'S STATIONERY OFFICE

Government Bookshops

49 High Holborn, London WC1V 6HB
13a Castle Street, Edinburgh EH2 3AR
41 The Hayes, Cardiff CF1 1JW
Brazennose Street, Manchester M60 8AS
Wine Street, Bristol BS1 2BQ
258 Broad Street, Birmingham B1 2HE
80 Chichester Street, Belfast BT1 4JY

Government publications are also available through booksellers